

# Semantically-Aware Attentive Neural Embeddings for Image-based Visual Localization

Zachary Seymour\*, Karan Sikka, Han-Pang Chiu, Supun Samarasekera, and Rakesh Kumar

SRI International, Princeton, NJ, USA

## Abstract

We present a novel method for fusing appearance and semantic information using visual attention for 2D image-based localization (2D-VL) across extreme changes in viewing conditions. Our deep learning based method is motivated by the intuition that specific scene regions remain stable in the semantic modality even in the presence of vast differences in the appearance modality. The proposed attention-based module learns to focus not only on discriminative visual regions for place recognition but also on consistently stable semantic regions to perform 2D-VL. We show the effectiveness of this model by comparing against state-of-the-art (SOTA) methods on several challenging localization datasets. We report an average absolute improvement of 19% over current SOTA 2D-VL methods. Furthermore, we present an extensive study demonstrating the effectiveness and contribution of each component of our model, showing 8%–15% absolute improvement from adding semantic information, and an additional 4% from our proposed attention module, over both prior methods as well as a competitive baseline.

## 1. Introduction

Accurately estimating the location from which a photo was taken in large-scale environments is crucial to applications in robotics [25, 45], augmented reality [25], virtual tourism [46], and autonomous navigation [12, 25, 30, 32, 34, 42]. This problem, also referred to as visual localization [25, 37, 42], needs to operate under changing conditions such as illumination (day/night), weather (sunny/snow), and seasons (summer/winter). Visual localization also needs to tackle dynamic scene changes and occlusions, such as road-work, pedestrians, and moving cars in urban cities [32, 60].

\*First author can be contacted at zachary.seymour@sri.com. Part of this work was done while the first author was an intern at SRI International and a student at Binghamton University, SUNY. He is currently a full-time employee at SRI International.

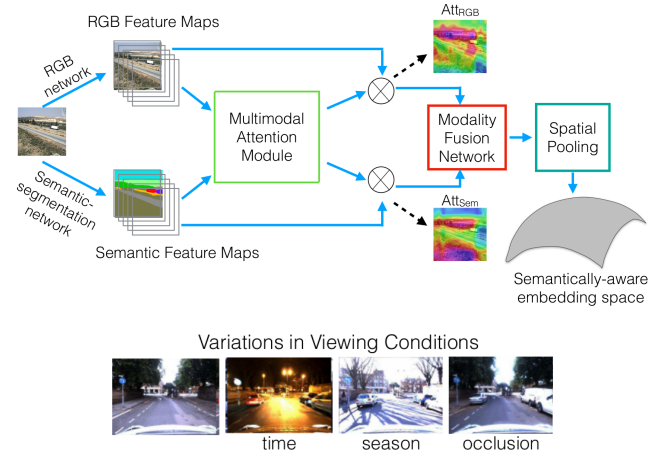


Figure 1: We show a high-level overview (top) of our approach (SAANE) that learns to effectively combine appearance and semantic information with modality-specific spatial attention to compute semantically-aware feature embeddings in the presence of severe changes in viewing conditions (bottom).

These requirements are integral for lifelong operation of an autonomous robotic agent [34].

Prior works on visual localization generally utilize two broad classes of methods: 3D structure-based localization (3D-VL) and 2D image-based localization (2D-VL) [41, 42]. Both methods typically rely on using local or global low-level appearance descriptors for pose estimation. 3D-VL methods typically associate a local descriptor with each point in a 3D model of the scene [23, 29, 40], while 2D-VL methods extract a holistic descriptor or multiple local descriptors for query-based matching [4, 5, 50, 51]. A primary drawback with methods using low-level features is that they are not robust to changes in viewing conditions [34, 43]; while 3D models are less scalable and present greater computational complexity. To this end, we focus on improving 2D-VL methods specifically for operating under severe changes in viewing conditions in large-scale urban environments and over large time lags [32].

Recently 2D-VL methods have achieved performance improvements by using deep convolutional neural networks (DCNN) based frameworks that learn to generate holistic image representation (or embeddings), that are invariant to viewing conditions [4, 21, 60]. Despite advancing the state-of-the-art, DCNN still suffer from two key issues in visual localization. First, due to the reliance on low or mid-level appearance features, DCNN methods suffer a loss in accuracy for large changes in viewing conditions such as viewpoint, weather, lighting [34, 43]. Second, since DCNN methods extract holistic representations from an entire image without any explicit understanding of scene composition, the resulting image representation is degraded by non-discriminative visual elements such as pedestrians and cars [34, 37, 60]. To alleviate these issues, we propose a novel DCNN framework to improve the robustness of learned visual embeddings by incorporating (i) high-level semantic information inside the neural network and (ii) an attention-based framework that uses both mid-level appearance and high-level semantic information to guide the model to focus on informative and stable image regions.

Our method, referred to as Semantically-Aware Attentive Neural Embeddings (SAANE) (see Figure 1), is an end-to-end trainable deep neural network, that effectively combines semantic<sup>1</sup> and mid-level appearance features with spatial attention to learn semantically-aware image embeddings. The design of SAANE is inspired by recent advances in deep multimodal and attention guided learning [1, 2, 52, 54, 55] and is composed of three key modules: (i) the *modality fusion module* that fuses information from the appearance and semantic input streams, (ii) the *multimodal attention module* that uses the fused representation to predict a shared channel attention and separate spatial attentions for the input modalities, and (iii) the *spatial pooling module* that pools the attended multimodal features to generate image embeddings, which are then used to retrieve matches for a query image. We use convolutional feature maps from models pre-trained for image classification and semantic segmentation as mid-level appearance and high-level semantic representations respectively. Our model is trained in an end-to-end manner by using a max-margin based triplet ranking loss function.

The key motivation behind our approach is that compared to low or mid-level appearance descriptors, the spatial layout of semantic classes in the image yields scene descriptions that have a higher invariance to large changes in viewing conditions for visual localization. The semantic understanding of the image content along with spatial attention helps to determine which regions of the scene may be unreliable for localization across time. Several prior works have attempted to improve the robustness of low-level features by using

ideas such as using GPS information to detect distracting patterns [18, 26], spatial attention [60], fusing semantic information inside local features [6], *etc.* A key advantage of SAANE over these earlier works is that it offers a principled end-to-end architecture to learn semantically-aware image representations with spatial attention, guided by multimodal features.

The key contributions of this paper are as follows:

1. We incorporate higher-level semantic information along with commonly-used mid-level appearance features to enhance the quality of (learned) image embeddings for visual localization under large appearance changes.
2. We propose two re-usable blocks using visual attention to guide the model to focus on stable and discriminative regions. To the best of our knowledge, ours is the first work to propose a DCNN-based pipeline that combines multimodal representation, from appearance and semantic information, with spatial attention for visual localization.
3. We perform comprehensive ablation studies and evaluation across several datasets and baselines to decompose the contribution of each part of our model. We particularly investigate and establish the necessity of separable spatial with shared channel attention to handle multimodal data.
4. We visualize the produced attention maps to provide useful insights in our algorithm. Finally, we show consistent improvements over the prior state-of-the-art.

## 2. Related Work

Methods for image-based visual localization generally fall into two classes: 3D structure-based localization (3D-VL) [40, 42, 43, 48, 57] and 2D image-based localization (2D-VL) [4, 14, 15, 50, 60]. 3D-VL methods create a 3D model of the scene by either using Structure-From-Motion (SfM) or associating local patches to 3D point clouds. On the other hand, 2D-VL methods formulate visual localization as an image retrieval problem by matching a query image with geo-tagged database images for approximate localization. An important benefit of 3D-VL methods is that they can estimate precise camera pose of the query as compared to 2D-VL methods; however, generating and maintaining a database of images in 2D-VL methods is simpler and more scalable for large-scale scenes. In this paper we focus on improving 2D-VL methods in large-scale scenes, which can then be used in combination with 3D methods for more precise localization as recently shown by Sattler *et al.* [42].

Most initial works for visual localization relied on matching Bag of Visual Word (BoVW)-type features [5, 20] or using global image descriptors in addition to sequential

<sup>1</sup>By *semantic* we refer to representations that provide high-level information about the input; *e.g.*, per-pixel depth or semantic segmentation maps.

search [33]. Building on the success of deep convolutional neural networks (DCNN) in other areas [19, 27], recent works have extensively demonstrated the effectiveness of off-the-shelf DCNN features for visual place recognition or localization [9, 18, 47]. Several works have also focused on improving feature pooling methods for off-the-shelf features [7, 50, 56] or those learned in end-to-end pipelines [4, 60].

We also situate our work within the space of making image features semantically-grounded and more robust to appearance changes. A typical approach to matching image features across large perceptual changes is to learn a transformation from one type of appearance to another, such as across seasons [35] or across different times of day [3, 31]. Gomez-Ojeda *et al.* [21] were one of the first to introduce directly training DCNNs for appearance invariance by leveraging synchronized route traversal data. Chen *et al.* show that training a DCNN on a parallel task—to match static locations across temporal or seasonal changes—produces features that perform better on localization tasks across appearance changes [8] and that focus on interesting image regions [10]. Our method seeks to integrate this innovation with stable semantic scene features to further improve the invariance of these features.

In general, (deep) learned global descriptors are more robust than hand-crafted features but are still susceptible to perceptual aliasing from repeated patterns such as road markings and buildings that introduce indistinguishable global matches; *i.e.*, only specific, meaningful regions are useful for localization [11, 16, 49]. Works such as SemanticSIFT [6] and LoST [18] encode spatial regions with off-the-shelf semantic features to strengthen the extracted features against perceptual aliasing. While our model also operates on the same core idea, we instead learn to effectively combine appearance and semantic features in a principled manner. In some prior work, the contribution of combining mid-level image features with higher-level semantic information has been entangled with the addition of 3D information [38, 43]. For example, Schönberger *et al.* [43] trains an end-to-end model, but the semantic information is used to encode LIDAR point clouds for performing 3D-VL. On the other hand, Naseer *et al.* [34] utilize a segmentation network to focus on geometrically-stable, man-made regions, such as buildings and poles; however, the region types are fixed, manually-selected, and then labeled manually. Our method’s novel multimodal attention module learns not only to combine features across modalities but also to focus on the most stable regions by discovering region types in a data-driven fashion.

### 3. Approach: SAANE

We now describe our approach, that we refer to as **SAANE** (Semantically-Aware Attentive Neural Embeddings), in detail. Our model uses an RGB image as input and

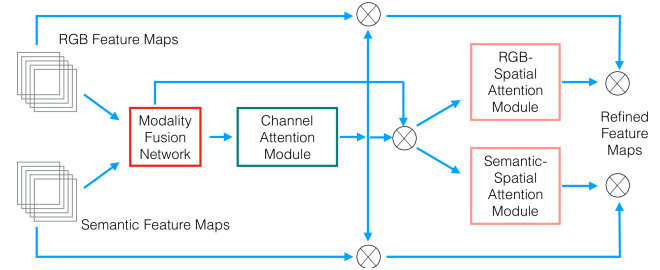


Figure 2: We provide an expanded view of the proposed Multi-modal Attention Module (MM-Att) that computes a shared channel attention and separated spatial attention for each modality.

passes it through two DCNNs pre-trained for image classification and semantic segmentation tasks. We use convolutional feature maps from the image classification network as mid-level appearance features (denoted as  $App_{mid}$ ) and from the semantic segmentation network as high-level semantic features (denoted as  $Sem_{high}$ ). We denote feature maps from an intermediate layer  $l$  of the image-classification and semantic-segmentation CNNs as  $F_l^A \in \mathbb{R}^{C_A \times H \times W}$  and  $F_l^S \in \mathbb{R}^{C_S \times H \times W}$  respectively, where  $C_A$  and  $C_S$  are the number of channels. We drop the notation  $l$  in the rest of the paper for brevity. We work in a supervised setting with a training set which consists of a database of images with their ground-truth location tags.

SAANE is an end-to-end trainable DCNN that learns to produce multimodal image embeddings that, in addition to being invariant to changes in viewing conditions, are aware of semantic composition of the scene and that focus explicitly on informative visual elements. Our model (Figure 1) consists of three NN-based modules: (i) the modality fusion module, (ii) the multimodal attention (MM-Att) module, and (iii) the spatial pooling module. SAANE operates by first transforming and fusing features from the appearance and the semantic input streams by using the modality fusion module. The output is a semantically-informed multimodal representation of input, which is then used to estimate per-modality spatial attentions using the proposed MM-Att module (Figure 2). The design of MM-Att module is motivated by Woo *et al.* [52], where attention was used to improve image classification for a unimodal (RGB) input. We adapt their model to work with multimodal inputs by computing a shared channel attention and using it to produce separate spatial attentions as described below. The output from this module is used to refine the feature maps from both modalities, which are then fused together with another modality fusion module. Finally, we use a spatial pooling step to output the embeddings. We train our model in an end-to-end fashion to learn each of these modules for visual localization. We now describe these modules along with the loss function and the training procedure.

**Modality Fusion Module.** The modality fusion module

aligns the feature maps— $App_{mid}$  and  $Sem_{high}$ —by first projecting them in a common space and then adding them together [2, 55]. We use  $1 \times 1$  convolutions, denoted by  $W_A^1 \in \mathbb{R}^{C \times C_A \times 1 \times 1}$  and  $W_S^1 \in \mathbb{R}^{C \times C_S \times 1 \times 1}$  for the appearance and semantic streams respectively, to project the feature maps in a common space.

$$\begin{aligned} F^M &= W_A^1 \circledast F^A + W_S^1 \circledast F^S \\ &= F_A^M + F_S^M, \end{aligned} \quad (1)$$

where  $F^M$  is the fused multimodal representation of the image,  $F_A^M$  and  $F_S^M$  are the aligned features maps from  $App_{mid}$  and  $Sem_{high}$  respectively,  $C$  is the number of channels in the common space, and  $\circledast$  is the convolutional operator. The output is a semantically-informed multimodal representation of the input and is used as input to both MM-Att and later to the spatial pooling module. Although more sophisticated fusion techniques *e.g.*, bilinear pooling have been used recently [17], we opted for projected sum pooling since it is easy to use, uses few trainable parameters, and also maintains the spatial configuration of the feature maps.

**Multimodal Attention Module (MM-Att).** The multimodal attention module (Figure 2) is responsible for predicting attention at different spatial locations independently for appearance and semantic input streams. The spatial attention allows our network to selectively focus on discriminative and stable image regions such as buildings or landmarks instead of confusing or dynamic elements such as sky, cars, and pedestrians [60]. This results in embeddings that are more robust to perceptual changes especially in urban environments. We extend the attention block recently proposed by Woo *et al.* [52] to use the combined multimodal representation, computed by the fusion module, to sequentially predict a shared channel attention (denoted by  $M_c \in \mathbb{R}^C$ ) and individual spatial attentions for the two modalities (denoted by  $M_{xy}^A \in \mathbb{R}^{H \times W}$  and  $M_{xy}^S \in \mathbb{R}^{H \times W}$  for appearance and semantic channels respectively). The channel attention is computed by summarizing the feature maps across the spatial dimensions by *average* ( $F_{avg}^M$ ) and *max* ( $F_{max}^M$ ) pooling, and passing them through a multi-layer perception (MLP) followed by an addition and a (sigmoid) non-linearity:

$$M_c = \sigma(\phi(F_{avg}^M) + \phi(F_{max}^M)), \quad (2)$$

where  $\sigma$  denotes the sigmoid function,  $\phi$  denotes a two-layer MLP shared across the two pooled inputs. The refined multimodal representation  $\hat{F}^M$  with attended channels is then computed by

$$\hat{F}^M = F \odot M_c, \quad (3)$$

where  $\odot$  denotes element-wise multiplication with appropriate broadcasting (copying) of attention values along the spatial dimension. The refined image representation is then

used to predict per modality spatial attentions by using two  $7 \times 7$  convolutional filters— $W_A^2$  and  $W_S^2$ —for appearance and semantic input streams, respectively.  $\hat{F}^M$  is pooled across the channel dimension by both *average* ( $\hat{F}_{avg}^M$ ) and *max* ( $\hat{F}_{max}^M$ ) pooling and concatenated across the channel dimension and convolved with the corresponding filters. The spatial attention maps are then used with the common channel attention to attend to the transformed maps from Equation 1 and generate refined features denoted as  $\hat{F}^A$  and  $\hat{F}^S$  for  $App_{mid}$  and  $Sem_{high}$ , respectively:

$$M_{xy}^A = M_c \odot \sigma(\hat{W}_A^2 \circledast ([\hat{F}_{avg}^M; \hat{F}_{max}^M])) \quad (4)$$

$$M_{xy}^S = M_c \odot \sigma(\hat{W}_S^2 \circledast ([\hat{F}_{avg}^M; \hat{F}_{max}^M])). \quad (5)$$

The final attended features  $\hat{F}^A$  and  $\hat{F}^S$  from the appearance and semantic input streams are given by

$$\hat{F}^A = F_A^M \odot M_{xy}^A \quad \hat{F}^S = F_S^M \odot M_{xy}^S. \quad (6)$$

We use another modality fusion module to fuse these refined features and then input them to the spatial pooling module. We later show the advantages of using a tied channel attention as a way to guide spatial attentions from both appearance and semantic information in §4.

**Spatial Pooling Module.** This module is responsible for pooling the information from the attended and fused features from the previous modules. In this work we use spatial pyramid pooling (SPP) [28] since it has been previously shown to be effective, and does not include any trainable parameters. We use SPP with pooling sizes of [4, 3, 2, 1] and concatenate the feature maps from all layers to produce the final embedding. Other equally effective alternatives to SPP, such as NetVLAD [4], would work in our framework. Finally, following the intuition of Ranjan *et al.* [39], we  $L_2$ -normalize these embeddings and scale them by a factor of  $\alpha = 10$ .

**Loss.** We use a max-margin-based triplet ranking loss function to learn our model [44]. This loss optimizes the network such that images from similar locations should be located closer in the embedding space than images from different locations. Formally, given an image  $I$ , a positive matching exemplar  $I_p$ , and a negative exemplar  $I_n$ , the loss is given by

$$\mathcal{L} = \max(0, m + d(\psi(I), \psi(I_p)) - d(\psi(I), \psi(I_n))), \quad (7)$$

where  $\psi$  denotes the embeddings produced by our model,  $m$  is the margin enforced between positive and negative exemplars, and  $d$  is some distance metric. For computational efficiency, we form triplets in an online manner by sampling them from each minibatch [44].



## 4. Experimental Results

In this section, we first briefly describe our training and testing datasets, along with our chosen evaluation metric (§4.1). We also provide details regarding the implementation of our model. Thereafter, we compare our model against a competitive DCNN baseline and rigorously evaluate the effects of each component of our model (§4.2). We then discuss several qualitative results to provide important insights regarding our proposed attention module (§4.3). Finally, we also compare our approach with previous state-of-the-art (SOTA) 2D-VL methods on the three test datasets (§4.4).

### 4.1. Datasets and Evaluation

**Training Dataset.** We utilize a version of the Specific Places Dataset (SPED) introduced by Chen *et al.* [8] to train our model. We randomly sample approximately 2600 cameras from the Archive of Many Outdoor Scenes [24] and download images collected every half hour from February and August 2014. We remove all images where the camera feed was corrupted, obscured, or too dark for visibility. We also remove images from any cameras for which the image capture location was not fixed. The final dataset comprises 1.3 million images drawn from 2079 cameras featuring significant scene diversity, ranging from urban roads to unpopulated landscapes, and significant appearance changes due to seasonal and day-night cycles. We train our model on this dataset and evaluate the performance on a visual localization task on three public datasets as described below.

**Nordland** [36] is derived from continuous video footage of a train journey recorded for a Norwegian television program,<sup>2</sup> recorded from the front car of the train across four different seasons. We extract one frame per second from the first hour of each traversal, excluding images where the train is either stopped or in tunnels. This results in 1403 frames per traversal. We perform our experiments by constructing a database with the summer traversal and querying it with the winter traversal (Sum.→Win.). The images feature no viewpoint variation, due to travel on fixed rails; however, the seasonal appearance changes are quite severe.

**St. Lucia** [20] comprises ten different traversals recorded by a forward-facing webcam affixed to the roof of a car, following a single route through the suburb of St. Lucia, Queensland, Australia. This dataset was captured at five different times of day on different days across two weeks. We use the first traversal ('100909\_0845') as the database and query with the remaining nine, reporting the average as well as the worst case result over the nine trials. We sample images at one frame per second, which results in each traversal containing on an average 1350 frames. The dataset features slight viewpoint variations due to differences

in the route taken by the vehicle. There are mild to moderate appearance changes due to differences in time of day and the presence of dynamic objects in the scene.

**Oxford RobotCar** [32] comprises several different traversals of the city of Oxford by a vehicle. It was collected across varying weather conditions, seasons, and times of day over a period of a year. We select two pairs of traversals, referred to as Overcast Autumn/Night Autumn and Overcast Summer/Snow Winter.<sup>3</sup> We perform an experiment by building a database with either Overcast Summer or Overcast Autumn and querying it with Snow Winter (Sum.→Win.) or Night Autumn (AM→PM), respectively. We make use of the center image from the front-facing camera and extract one frame per second. On average, each traversal covers nearly 9 km and 2000 frames. There are mild viewpoint variations present, again due to slight differences in the starting point and road position of the traversals. The appearance change in the day-night pair is quite drastic, largely from the difference in illumination quality in the transition from sunlight to street lights; while it is more moderate in the summer-winter pair, with minor variation from seasonal vegetation and ground cover.

**Evaluation Metric.** We report our results as Area Under the Curve (AUC) by constructing precision-recall curves using “the ratio test” [47]. In brief, a match between a query image and the database is considered positive if the ratio of the Euclidean distances of the best match and the second-best match by nearest neighbor search is above some threshold, and a negative match otherwise. Because every frame in the test datasets has a ground truth matching frame (*i.e.*, there are no true negatives), every negative reported by the ratio test is a false negative. A match is a true positive if it is within 5 frames of the ground truth and a false positive otherwise.<sup>4</sup> A precision-recall curve is constructed by varying the threshold on the ratio test. We do not use any priors or post-processing such as sequential information in selecting the matches, as all nearest neighbors-based image retrieval methods could be enhanced by such techniques.

**Implementation Details.** The backbone of SAANE is two parallel DCNNs. We use a ResNet50 [22] pre-trained for the Imagenet classification task for mid-level feature extraction and a Pyramid Scene Parsing Network (PSPNet) [58] pre-trained on the ADE20K [59] semantic segmentation task for extracting semantic features. We also experimented with a version of PSPNet pre-trained on Cityscapes [13]; however, we found the ADE20K version to be more robust to view-

<sup>3</sup>The first three were introduced in [18], and the traversals were originally referred to in [32] as 2014-12-09-13-21-02, 2014-12-10-18-10-50, 2015-05-19-14-06-38, and 2015-02-03-08-45-10, respectively.

<sup>4</sup>For Nordland, we use the synchronized frame correspondence. On the other test datasets, 5 frames covers the ground-truth frame variance (0–25 m), a stricter requirement for positive localization than is typically used for place recognition (25–40 m). See Appendix A for a detailed discussion.

<sup>2</sup><https://nrkbeta.no/2013/01/15/nordlandsbanen-minute-by-minute-season-by-season/>

Method	Semantic	Individual Attention	Multimodal Attention	Nordland Sum. $\rightarrow$ Win.	St. Lucia Average	Worst	RobotCar AM $\rightarrow$ PM	RobotCar Sum. $\rightarrow$ Win.
App [Baseline]				58.0	71.4	55.5	36.6	79.6
App+Sem	✓			74.6	74.9	60.6	61.4	87.9
App-Att		✓		74.2	74.0	60.3	60.9	86.5
App-Att+Sem-Att	✓	✓		68.5	73.9	58.9	62.9	83.6
SAANE [Proposed]	✓		✓	<b>77.3</b>	<b>78.3</b>	<b>69.1</b>	<b>67.3</b>	<b>88.5</b>
DenseVLAD [50]				19.2	64.5	35.5	22.9	78.6
NetVLAD [4]				36.7	57.7	33.1	37.0	86.8
AMOSNet* [8]				45.6	75.3	63.7	45.3	75.1
APANet* [60]		†		27.0	42.4	26.1	11.2	58.2
APANet-MM* [60]	✓	†		24.9	41.2	23.0	16.4	58.3

Table 1: Evaluation results of the different models discussed in §4.2 and §4.4. We report area under the precision-recall curve (AUC) for each method. We show results with prior state-of-the-art models below the double line. \* denotes models that we implemented and trained on SPED dataset that was used to train our model. † denotes variants of spatial attention that are distinct from our proposed method.

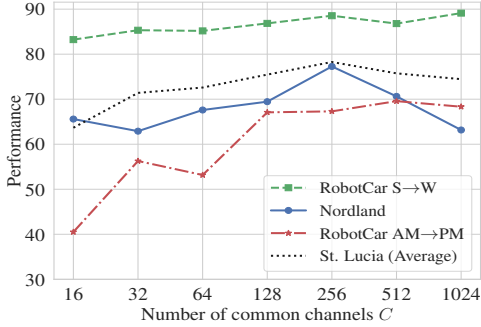


Figure 3: Figure shows a plot of performance of SAANE versus the number of channels  $C$  in the common embedding space as computed in Equation 1.

point changes and the 150 classes of ADE20K to be more useful in the presence of diverse scene types. We use the output of the third residual block from ResNet50 as mid-level appearance features ( $F^A$ ). For high-level semantic features ( $F^S$ ), we use the output before the final convolutional layer of PSPNet. The resulting number of channels in appearance and semantic features are  $C_R = 1024$  and  $C_S = 512$ , respectively. We set the number of channels of the common embedding space in the modality fusion module ( $C$ ), both before and after MM-Att, to 256. The dimensionality of the final embeddings after spatial pooling is 7680. For our experiments, we use the two pre-trained DCNNs and fine-tune the two modality fusion modules and the MM-Att module. We use the Adam optimizer with a learning rate  $5 \times 10^{-5}$  and weight decay of  $5 \times 10^{-4}$  for training. We use online triplet sampling with batches comprised of 16 different classes with 4 examples per class. Within a batch, we utilize distance-weighted triplet sampling [53] to increase the stability of the training process. We use a margin of  $m = 0.5$ , selected based on giving the best performance on a small validation set. Finally, due to our assumption that our test data come from a dissimilar distribution as our training data, we did not

experiment with any form of whitening as used in [4, 60].

**Prior Methods.** For a fair comparison with prior methods, we use the same backbone DCNN—pre-trained ResNet50—for all methods. We implement AMOSNet [8] by fine-tuning all layers of the pre-trained DCNN on the SPED dataset. We also implement a recent SOTA method using both attention and pyramid pooling, Attention-based Pyramid Aggregation Network (APANet) [60]. We first implement their proposed cascade pyramid attention block over the deep appearance features. Although their method did not utilize semantic information, we also experiment with a stronger baseline by using two cascade pyramid attention blocks over the output feature maps of each of our backbone networks (plus our initial multimodal projection as in Equation 1). We use the learned attention to sum pool the spatial pyramid features and then sum the two modalities to achieve the final embedding. We also compare with implementations of DenseVLAD [50] and NetVLAD [4], trained on the Pitts30k visual place recognition dataset [51], provided by the respective authors. We attempted to train a NetVLAD-based network similar to APANet but found that the model converged poorly on the SPED dataset; thus, we present the results achieved using the pre-trained weights.

## 4.2. Quantitative Results

The performance of the proposed method along with different baselines and prior SOTA approaches is presented in Table 1. We first compare our model with different baselines to highlight the benefits of the proposed ideas: (i) use of semantic information, and (ii) use of a novel multimodal attention module to focus on discriminative regions.

To validate the benefits of semantic information, we first compare the performance of the baseline model using only appearance information (App [Baseline]) with that using both appearance and semantic information (App+Sem). Across our test datasets, there is an average increase in absolute performance from introducing the semantic informa-

tion of 9%, with the largest gain (25%) on the RobotCar AM→PM trial. Nordland shows the second-largest improvement (17%) from multimodal fusion. We also note that the improvement is similar with App-Att, indicating that both attention and the semantic modality help to compensate for the extreme perceptual aliasing compared to the (sub)urban traversal datasets.

The remaining variants (App-Att, App-Att+Sem-Att, and SAANE) serve to demonstrate the benefits of the proposed attention modules. Between App [Baseline] and App-Att, we see an increase in performance (8% average absolute on all datasets) from the attention module causing the model to focus on less confusing regions. The improvements on Nordland (16%) from attention alone demonstrate how the module suppresses confusing regions. We observe less improvement on St. Lucia (3%) because of the relatively smaller appearance variations present across traversals. This increase across all datasets demonstrates that introducing spatial attention with appearance information results in performance gains.

However, this does not seem to be the case if we naively compute attention from both modalities with separate channel and spatial attention. For example, while comparing App-Att+Sem-Att—the model variant that predicts separate attention over each modality—with App+Sem, we observe only minor improvements on the RobotCar AM→PM dataset (2%). These observations seem to demonstrate that attention is useful for suppressing confusing regions from both the appearance and semantic modalities.

Our model tackles this problem by using the fused multimodal image representation to predict spatial attention for each modality by first predicting an intermediate shared channel attention. SAANE yields the best performance across all variants on each dataset (12% average absolute improvement over the baseline and 4% over App+Sem and 5% over App-Att+Sem-Att). Both Nordland (9%) and St. Lucia (11% in the worst case) are further refined by sharing channel attention across modalities, while the most perceptually-challenging test, RobotCar AM→PM, sees a further performance increase of 4% over App-Att+Sem-Att and of 31% over App [Baseline]. In summary our model shows consistent improvements over different baselines across all datasets for the task of visual localization.

Finally, to explore the effect of the model capacity on performance on the test datasets, we experiment with varying the dimensionality  $C$  of the multimodal fusion network (Equation 1). As shown in Figure 3, the performance across all of the datasets plateaus between 128 and 256 channels and shows evidence of overfitting, particularly in the case of Nordland, above 256 channels. The best dimensionality of the multimodal fusion module also appears to be a function of the dataset difficulty. Our model’s performance on RobotCar Sum.→Win., in the presence of minor seasonal

variations, is relatively stable, even down to 16 channels, while the tasks with more extreme variation, such as RobotCar AM→PM, sharply decline below 128.

### 4.3. Qualitative Results

In Figure 4, we present top retrievals for two cases with significant variations in viewing conditions. We visualize where our model attends by showing the spatial attention maps from both modalities along with the semantic segmentation maps. The top two rows (Figure 4a) show a query image from the Night Autumn matched against retrieved database images from the Overcast Autumn set of Oxford RobotCar (*i.e.*, AM→PM in Table 1). For methods relying only on appearance information (*i.e.*, AMOSNet and the baseline), the retrieved images in the rightmost column are incorrect but present similar scene layouts, while our model retrieves a match within two meters of the query location. We see that across time of day, the maps from both attention modalities remain consistent and focus on stable features, with the appearance attention focusing mostly on fine details such as lane markings or architectural elements and semantic attention giving emphasis to scene layout and skyline shape. Interestingly, we note the bus present in the matched database image, obscuring a significant part of the scene. While the appearance modality attends highly to the bus’s features, as if it were any other structure, we can see that the semantic attention module has learned to disregard this region as a dynamic object and give more emphasis to the remaining scene layout.

In the third and fourth rows (Figure 4b), we show an example from the Nordland task, with the database constructed using the summer sequence and querying with an image from the winter sequence. Here, we also compare against our App+Sem model, combining both modalities without attention. At a quick glance, the image retrieved using AMOSNet is nearly indistinguishable from the correct match; however it lacks the distinctive fence structure to the left of the image that our appearance attention module focuses highly on in both seasons. In the case of the match from App+Sem, the match is nearly correct, within a few frames of the query image. This also demonstrates the capacity of the attention module to further refine the predicted pose to provide a much more accurate localization. We conclude that the learned attention module forces our model to look at consistent regions even across extreme changes in viewing conditions.

### 4.4. Comparison with state-of-the-art

Table 1 shows the comparison of our model with several SOTA techniques. Our model shows obvious improvements on the test datasets in comparison to DenseVLAD (28% average absolute) and NetVLAD (19%), both SOTA 2D-VL methods. We note that NetVLAD performs comparably to



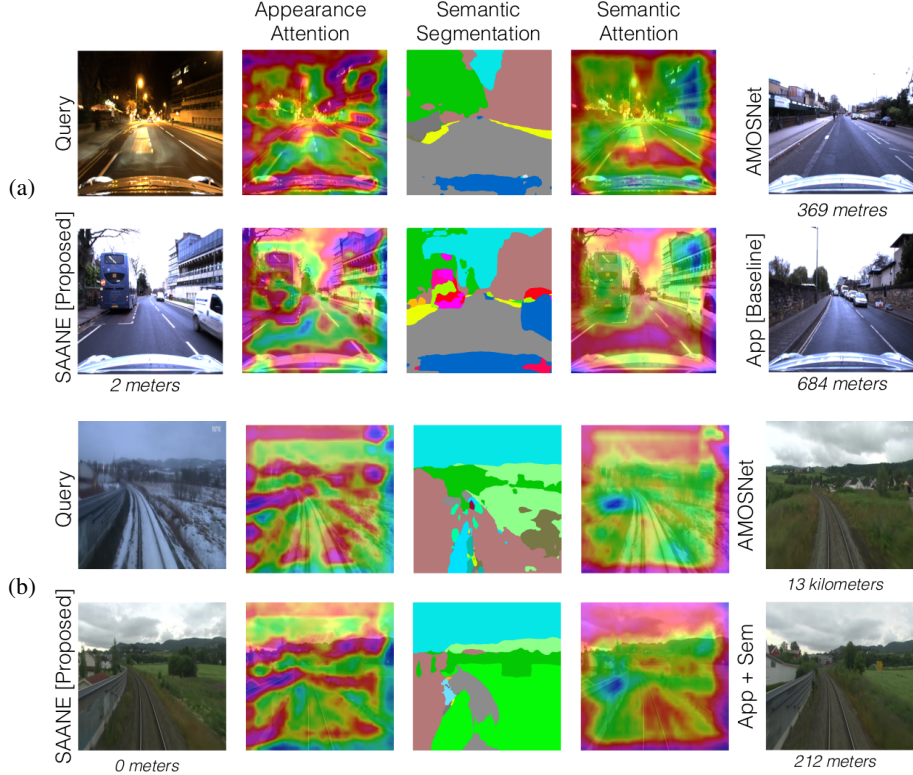


Figure 4: We present retrieval results for two examples under challenging appearance variations from (a) RobotCar AM→PM, and (b) Nordland, to evaluate the quality of our model and visualize the attention maps. We show a query image, database image retrieved using different methods, predicted attention maps, and the pre-computed semantic segmentation. The figure highlights that our model is able to retrieve the correct sample with and also produces attention maps that are consistent across extreme appearance changes. The palette for semantic segmentation is derived from ADE20K, as follows: skyscraper, sky, building, tree, wall, grass, sidewalk, car, plant, person, earth, fence, signboard, pole, streetlight, truck, conveyor, mountain, floor, van. Figure best viewed in color.

our model on RobotCar Sum.→Win. where the appearance changes are relatively minor; however, its performance is much lower on the test datasets with more extreme changes, which is consistent with prior work [18, 43]. We also observe an average absolute improvement of 12% (across all datasets) over AMOSNet, which was the previous SOTA method on both the Nordland and St. Lucia datasets. We note that the performance improvements over the appearance baseline for both our model and AMOSNet seem to be proportional to the amount of appearance variations present in the dataset. For example, on the St. Lucia dataset, which presents minor appearance variation, nearly the same result is achieved from fine-tuning on SPED (AMOSNet) as from adding additional semantic features (App+Sem). However, the capacity of our complete (SAANE) attention module to further refine the localization is shown again, with 3% improvement over AMOSNet. For cases with more severe appearance variation, we see a much larger improvement from training the proposed modules combining semantics, modality-specific spatial attention, and shared channel attention; *e.g.*, results on the Nordland dataset show an absolute improvement of 32% and on RobotCar AM→PM an improvement of 22%.

Similarly, SAANE also shows improvements between 37% and 38% over both implementations of APANet. Adding the semantic modality to APANet-MM is insufficient to significantly boost the performance of this pooling method in this scenario. From this, we conclude that directly using pyramid pooling on the multimodal feature maps is insufficient and that our method of first applying attention over the DCNN feature maps followed by pyramid pooling is superior.

## 5. Conclusion

We present an attention-based semantically-aware deep embedding model, called SAANE, for image-based visual localization in large-scale environments. Our model targets the sensitivity of appearance-based visual localization to both perceptual aliasing from repetitive structures and extreme differences in viewing conditions. SAANE uses a novel multimodal attention module that first fuses features from both modalities with shared channel attention to combine mid-level appearance cues with high-level semantic cues in a principled manner. It then predicts separate spatial attention maps for each modality before re-fusing them to induce the final joint embedding. We evaluate the performance benefits



of our model on three challenging public visual localization datasets, while showing significant gains compared to the baseline (12%). We also show that SAANE learns to produce stable attention maps that focus on consistent image regions across changing views. Finally, we demonstrate that the performance of our proposed approach is significantly superior to that of prior methods.

## 6. Acknowledgement

We would like to thank Ajay Divakaran for proof-reading the manuscript and providing helpful comments.

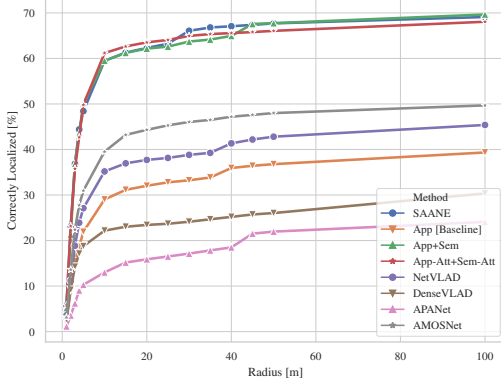
## References

- [1] T. Afouras, J. S. Chung, A. Senior, O. Vinyals, and A. Zisserman. Deep audio-visual speech recognition. *arXiv preprint arXiv:1809.02108*, 2018. [2](#)
- [2] K. Ahuja, K. Sikka, A. Roy, and A. Divakaran. Understanding visual ads by aligning symbols and objects using co-attention. *arXiv preprint arXiv:1807.01448*, 2018. [2](#), [4](#)
- [3] A. Anosheh, T. Sattler, R. Timofte, M. Pollefeys, and L. Van Gool. Night-to-day image translation for retrieval-based localization. *arXiv preprint arXiv:1809.09767*, 2018. [3](#)
- [4] R. Arandjelovic, P. Gronat, A. Torii, T. Pajdla, and J. Sivic. NetVLAD: CNN architecture for weakly supervised place recognition. In *CVPR*, pages 5297–5307, 2016. [1](#), [2](#), [3](#), [4](#), [6](#)
- [5] R. Arandjelović and A. Zisserman. DisLocation: Scalable descriptor distinctiveness for location recognition. In *ACCV*, pages 188–204, 2014. [1](#), [2](#)
- [6] R. Arandjelović and A. Zisserman. Visual vocabulary with a semantic twist. In *ACCV*, pages 178–195, 2014. [2](#), [3](#)
- [7] A. Babenko and V. Lempitsky. Aggregating local deep features for image retrieval. In *ICCV*, pages 1269–1277, 2015. [3](#)
- [8] Z. Chen, A. Jacobson, N. Sünderhauf, B. Upcroft, L. Liu, C. Shen, I. Reid, and M. Milford. Deep learning features at scale for visual place recognition. In *ICRA*, pages 3223–3230, 2017. [3](#), [5](#), [6](#)
- [9] Z. Chen, O. Lam, A. Jacobson, and M. Milford. Convolutional neural network-based place recognition. *arXiv preprint arXiv:1411.1509*, 2014. [3](#)
- [10] Z. Chen, L. Liu, I. Sa, Z. Ge, and M. Chli. Learning context flexible attention model for long-term visual place recognition. *IEEE Robotics and Automation Letters*, 3(4):4015–4022, 2018. [3](#)
- [11] Z. Chen, F. Maffra, I. Sa, and M. Chli. Only look once, mining distinctive landmarks from convnet for visual place recognition. In *IROS*, pages 9–16, 2017. [3](#)
- [12] G. Chowdhary, E. N. Johnson, D. Magree, A. Wu, and A. Shein. GPS-denied indoor and outdoor monocular vision aided navigation and control of unmanned aircraft. *Journal of Field Robotics*, 30(3):415–438, 2013. [1](#)
- [13] M. Cordts, M. Omran, S. Ramos, T. Rehfeld, M. Enzweiler, R. Benenson, U. Franke, S. Roth, and B. Schiele. The Cityscapes dataset for semantic urban scene understanding. In *CVPR*, 2016. [5](#)
- [14] M. Cummins and P. Newman. FAB-MAP: Probabilistic localization and mapping in the space of appearance. *The International Journal of Robotics Research*, 27(6):647–665, 2008. [2](#)
- [15] M. Cummins and P. Newman. Appearance-only SLAM at large scale with FAB-MAP 2.0. *The International Journal of Robotics Research*, 30(9):1100–1123, 2011. [2](#)
- [16] C. Finn, X. Y. Tan, Y. Duan, T. Darrell, S. Levine, and P. Abbeel. Deep spatial autoencoders for visuomotor learning. In *ICRA*, pages 512–519, 2016. [3](#)
- [17] A. Fukui, D. H. Park, D. Yang, A. Rohrbach, T. Darrell, and M. Rohrbach. Multimodal compact bilinear pooling for visual question answering and visual grounding. *arXiv preprint arXiv:1606.01847*, 2016. [4](#)
- [18] S. Garg, N. Suenderhauf, and M. Milford. LoST? appearance-invariant place recognition for opposite viewpoints using visual semantics. *Proceedings of Robotics: Science and Systems XIV*, 2018. [2](#), [3](#), [5](#), [8](#)
- [19] R. Girshick. Fast R-CNN. In *ICCV*, pages 1440–1448, 2015. [3](#)
- [20] A. J. Glover, W. P. Maddern, M. J. Milford, and G. F. Wyeth. FAB-MAP + RatSLAM: Appearance-based SLAM for multiple times of day. In *ICRA*, pages 3507–3512, 2010. [2](#), [5](#)
- [21] R. Gomez-Ojeda, M. Lopez-Antequera, N. Petkov, and J. Gonzalez-Jimenez. Training a convolutional neural network for appearance-invariant place recognition. *arXiv preprint arXiv:1505.07428*, 2015. [2](#), [3](#)
- [22] K. He, X. Zhang, S. Ren, and J. Sun. Deep residual learning for image recognition. In *CVPR*, pages 770–778, 2016. [5](#)
- [23] A. Irschara, C. Zach, J.-M. Frahm, and H. Bischof. From structure-from-motion point clouds to fast location recognition. In *CVPR*, pages 2599–2606, 2009. [1](#)
- [24] N. Jacobs, N. Roman, and R. Pless. Consistent temporal variations in many outdoor scenes. In *CVPR*, pages 1–6, 2007. [5](#)
- [25] A. Kendall, M. Grimes, and R. Cipolla. PoseNet: A convolutional network for real-time 6-DOF camera relocalization. In *ICCV*, pages 2938–2946, 2015. [1](#)
- [26] J. Knopp, J. Sivic, and T. Pajdla. Avoiding confusing features in place recognition. In *ECCV*, pages 748–761, 2010. [2](#)
- [27] A. Krizhevsky, I. Sutskever, and G. E. Hinton. Imagenet classification with deep convolutional neural networks. In *NIPS*, pages 1097–1105, 2012. [3](#)
- [28] S. Lazebnik, C. Schmid, and J. Ponce. Beyond bags of features: Spatial pyramid matching for recognizing natural scene categories. In *CVPR*, pages 2169–2178, 2006. [4](#)
- [29] Y. Li, N. Snavely, D. Huttenlocher, and P. Fua. Worldwide pose estimation using 3D point clouds. In *ECCV*, pages 15–29, 2012. [1](#)
- [30] H. Lim, S. N. Sinha, M. F. Cohen, and M. Uyttendaele. Real-time image-based 6-DOF localization in large-scale environments. In *CVPR*, pages 1043–1050, 2012. [1](#)
- [31] S. Lowry, M. Milford, and G. Wyeth. Transforming morning to afternoon using linear regression techniques. In *ICRA*, pages 3950–3955, 2014. [3](#)
- [32] W. Maddern, G. Pascoe, C. Linegar, and P. Newman. 1 year, 1000 km: The Oxford RobotCar dataset. *The International Journal of Robotics Research*, 36(1):3–15, 2017. [1](#), [5](#)
- [33] M. J. Milford and G. F. Wyeth. SeqSLAM: Visual route-based navigation for sunny summer days and stormy winter nights.

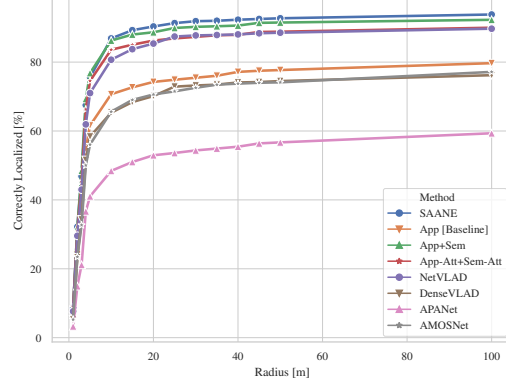
- In *ICRA*, pages 1643–1649, 2012. 3
- [34] T. Naseer, G. L. Oliveira, T. Brox, and W. Burgard. Semantics-aware visual localization under challenging perceptual conditions. In *ICRA*, pages 2614–2620, 2017. 1, 2, 3
- [35] T. Naseer, L. Spinello, W. Burgard, and C. Stachniss. Robust visual robot localization across seasons using network flows. In *AAAI*, pages 2564–2570, 2014. 3
- [36] P. Neubert, N. Sünderhauf, and P. Protzel. Superpixel-based appearance change prediction for long-term navigation across seasons. *Robotics and Autonomous Systems*, 69:15–27, 2015. 5
- [37] N. Piasco, D. Sidibé, C. Demonceaux, and V. Gouet-Brunet. A survey on visual-based localization: On the benefit of heterogeneous data. *Pattern Recognition*, 74:90–109, 2018. 1, 2
- [38] N. Radwan, A. Valada, and W. Burgard. VLocNet++: Deep multitask learning for semantic visual localization and odometry. *arXiv preprint arXiv:1804.08366*, 2018. 3
- [39] R. Ranjan, C. D. Castillo, and R. Chellappa.  $L_2$ -constrained softmax loss for discriminative face verification. *arXiv preprint arXiv:1703.09507*, 2017. 4
- [40] T. Sattler, M. Havlena, F. Radenovic, K. Schindler, and M. Pollefeys. Hyperpoints and fine vocabularies for large-scale location recognition. In *ICCV*, pages 2102–2110, 2015. 1, 2
- [41] T. Sattler, W. Maddern, C. Toft, A. Torii, L. Hammarstrand, E. Stenborg, D. Safari, M. Okutomi, M. Pollefeys, J. Sivic, et al. Benchmarking 6DOF outdoor visual localization in changing conditions. In *CVPR*, 2018. 1
- [42] T. Sattler, A. Torii, J. Sivic, M. Pollefeys, H. Taira, M. Okutomi, and T. Pajdla. Are large-scale 3D models really necessary for accurate visual localization? In *CVPR*, pages 6175–6184, 2017. 1, 2
- [43] J. L. Schönberger, M. Pollefeys, A. Geiger, and T. Sattler. Semantic visual localization. In *CVPR*, 2018. 1, 2, 3, 8
- [44] F. Schroff, D. Kalenichenko, and J. Philbin. Facenet: A unified embedding for face recognition and clustering. In *CVPR*, pages 815–823, 2015. 4
- [45] S. Se, D. Lowe, and J. Little. Mobile robot localization and mapping with uncertainty using scale-invariant visual landmarks. *The international Journal of robotics Research*, 21(8):735–758, 2002. 1
- [46] N. Snavely, S. M. Seitz, and R. Szeliski. Modeling the world from internet photo collections. *International journal of computer vision*, 80(2):189–210, 2008. 1
- [47] N. Sünderhauf, S. Shirazi, F. Dayoub, B. Upcroft, and M. Milford. On the performance of convnet features for place recognition. In *IROS*, pages 4297–4304, 2015. 3, 5
- [48] L. Svärm, O. Enqvist, F. Kahl, and M. Oskarsson. City-scale localization for cameras with known vertical direction. *IEEE transactions on pattern analysis and machine intelligence*, 39(7):1455–1461, 2017. 2
- [49] G. Tolias, R. Sivic, and H. Jégou. Particular object retrieval with integral max-pooling of CNN activations. *arXiv preprint arXiv:1511.05879*, 2015. 3
- [50] A. Torii, R. Arandjelovic, J. Sivic, M. Okutomi, and T. Pajdla. 24/7 place recognition by view synthesis. In *CVPR*, pages 1808–1817, 2015. 1, 2, 3, 6
- [51] A. Torii, J. Sivic, T. Pajdla, and M. Okutomi. Visual place recognition with repetitive structures. In *CVPR*, pages 883–890, 2013. 1, 6
- [52] S. Woo, J. Park, J.-Y. Lee, and I. S. Kweon. CBAM: Convolutional block attention module. In *ECCV*, 2018. 2, 3, 4
- [53] C.-Y. Wu, R. Manmatha, A. J. Smola, and P. Krähenbühl. Sampling matters in deep embedding learning. In *ICCV*, 2017. 6
- [54] H. Xu and K. Saenko. Ask, attend and answer: Exploring question-guided spatial attention for visual question answering. In *ECCV*, pages 451–466, 2016. 2
- [55] Z. Yang, X. He, J. Gao, L. Deng, and A. Smola. Stacked attention networks for image question answering. In *CVPR*, pages 21–29, 2016. 2, 4
- [56] J. Yue-Hei Ng, F. Yang, and L. S. Davis. Exploiting local features from deep networks for image retrieval. In *CVPR workshops*, pages 53–61, 2015. 3
- [57] B. Zeisl, T. Sattler, and M. Pollefeys. Camera pose voting for large-scale image-based localization. In *ICCV*, pages 2704–2712, 2015. 2
- [58] H. Zhao, J. Shi, X. Qi, X. Wang, and J. Jia. Pyramid scene parsing network. In *CVPR*, pages 2881–2890, 2017. 5
- [59] B. Zhou, H. Zhao, X. Puig, S. Fidler, A. Barriuso, and A. Torralba. Scene parsing through ADE20K dataset. In *CVPR*, 2017. 5
- [60] Y. Zhu, J. Wang, L. Xie, and L. Zheng. Attention-based pyramid aggregation network for visual place recognition. In *ACM MM*, pages 99–107, 2018. 1, 2, 3, 4, 6

## 7. Appendix

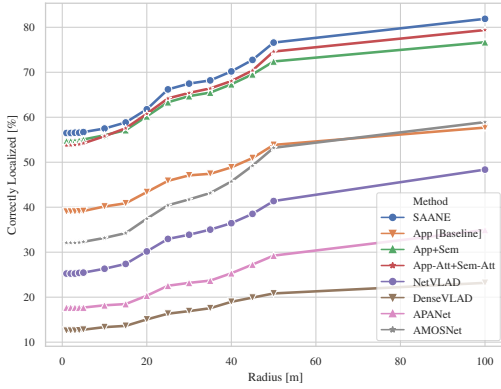
### 7.1. Localization Results



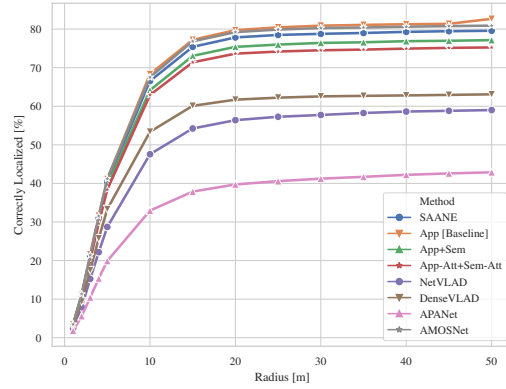
(a) RobotCar AM→PM



(b) RobotCar Sum.→Win.



(c) Nordland



(d) St. Lucia (Average)

Figure 5: We compare localization results from several different methods on each of our datasets by varying the match radius; *i.e.*, the top match by nearest neighbor search is considered correctly localized if it is within  $n$  meters of the ground truth location. Note: because the Nordland dataset is perfectly synchronized (unlike the others), the recall is already very high at  $<1\text{m}$ .

To better understand the performance of various methods across our test datasets, we drop the ratio test explained in §4.1 and present correct localization at a given radius. That is, the top-retrieved result by nearest neighbor search is considered correctly localized if it occurs within  $n$  meters of the ground truth, and incorrect otherwise. The results of our experiments in varying the value of  $n$  are presented in Figure 5. We can see that across varying radii, our results from Table 1 remain mostly consistent. As the threshold for correct localization becomes looser in the case of RobotCar AM→PM, App+Sem overtakes App+Att+Sem+Att and begins to converge with SAANE. In the Sum.→Win. case, we also see NetVLAD converge with App+Att+Sem+Att, which supports our analysis above that NetVLAD works quite well in scenarios with less variation in view conditions. Surprisingly, the same does not hold for St. Lucia, despite the relatively minor appearance variations; however, this may be a result of the lower quality camera with which the videos were collected.

### 7.2. Attended Semantic Classes

In order to achieve a better, quantitative understanding of where our attention module focuses in the image, we experiment with upsampling the predicted spatial attention maps and overlaying them on the pre-computed semantic segmentation. We select the cell in the  $14 \times 14$  attention map with the highest value and count the corresponding label values predicted by

$App_{mid}$		$Sem_{high}$	
Class	Frequency	Class	Frequency
building	59.9%	building	38.3%
sky	14.8%	road	16.4%
tree	5.9%	car	11.6%
road	5.1%	sky	6.0%
car	3.8%	sidewalk	5.7%
wall	2.1%	tree	4.9%
signboard	2.1%	signboard	2.7%
ceiling	1.2%	wall	2.7%
sidewalk	0.9%	traffic	1.7%
traffic	0.9%	person	1.2%
truck	0.5%	bus	1.2%
person	0.5%	rock	1.0%
marquee	0.3%	van	0.8%
bus	0.3%	truck	0.8%
earth	0.3%	river	0.8%
pole	0.2%	ceiling	0.5%
plant	0.2%	grass	0.5%
floor	0.2%	fence	0.5%
light	0.2%	earth	0.3%
fountain	0.2%	bicycle	0.3%
house	0.2%	sconce	0.2%
fence	0.2%	streetlight	0.2%

Table 2: To better understand the operation of our attention module, we present the classes most frequently attended to by the spatial map from each modality on RobotCar Sum.→Win. We calculate these by upsampling the highest value cell in the  $14 \times 14$  attention map and counting the pixels from the corresponding semantic segmentation output by PSPNet. Class names are taken from ADE20K.

PSPNet. The results of this experiment, computed on the combined database and query traversals of RobotCar Sum.→Win., are presented in [Table 2](#). We show the top represented classes along with their respective frequencies. While the frequencies from each modality follow a long-tail distribution, there is a much sharper drop between the first- and second-most attended class in the appearance modality than in the semantic modality. These results corroborate our analysis in [§4.3](#): the appearance branch of MM-Att tends to focus on buildings and architectural features nearly 60% of the time and, to a lesser extent, distinctive vegetation (6%) or road markings (5%). We expect most of the reports of the “sky” class come from overlaps with “building” due to spatial pooling. In the semantic modality, “building” is also the most-frequently attended class, though to a lesser extent than in the appearance modality. The frequency of “road” (16% also supports our analysis that the semantic spatial attention focuses on regions meaningful to scene layout; again, the frequency of “car” (12%) is likely explained by overlap with “road” from the DCNN spatial pooling.

### 7.3. Additional Visualizations

In [Figure 6](#), we present some additional retrieval results and visualization of our learned attention maps, as in [§4.3](#). We show results from RobotCar Sum.→Win. ([Figure 6a](#)) and St. Lucia ([Figures 6b](#) and [6c](#)). Of note is the failure case presented in [Figure 6c](#). In this case, both of our methods, SAANE and App+Sem, fail entirely, while AMOSNet retrieves a near-perfect match. In the case of App+Sem, the poor localization is likely due to the similarity of the semantic layout of the query image and the retrieved database match; *i.e.*, this match would normally be corrected by the attention module. However, the appearance attention of the query image shows a failure of our attention module: the shadow of the power pole cast across the road in the query image is strongly attended by MM-Att. As a result, a database image with a similar structure (perhaps a crosswalk) is retrieved, when instead the shadow should have been ignored. This may be indicative that not enough weight is being given to the semantic spatial attention branch.



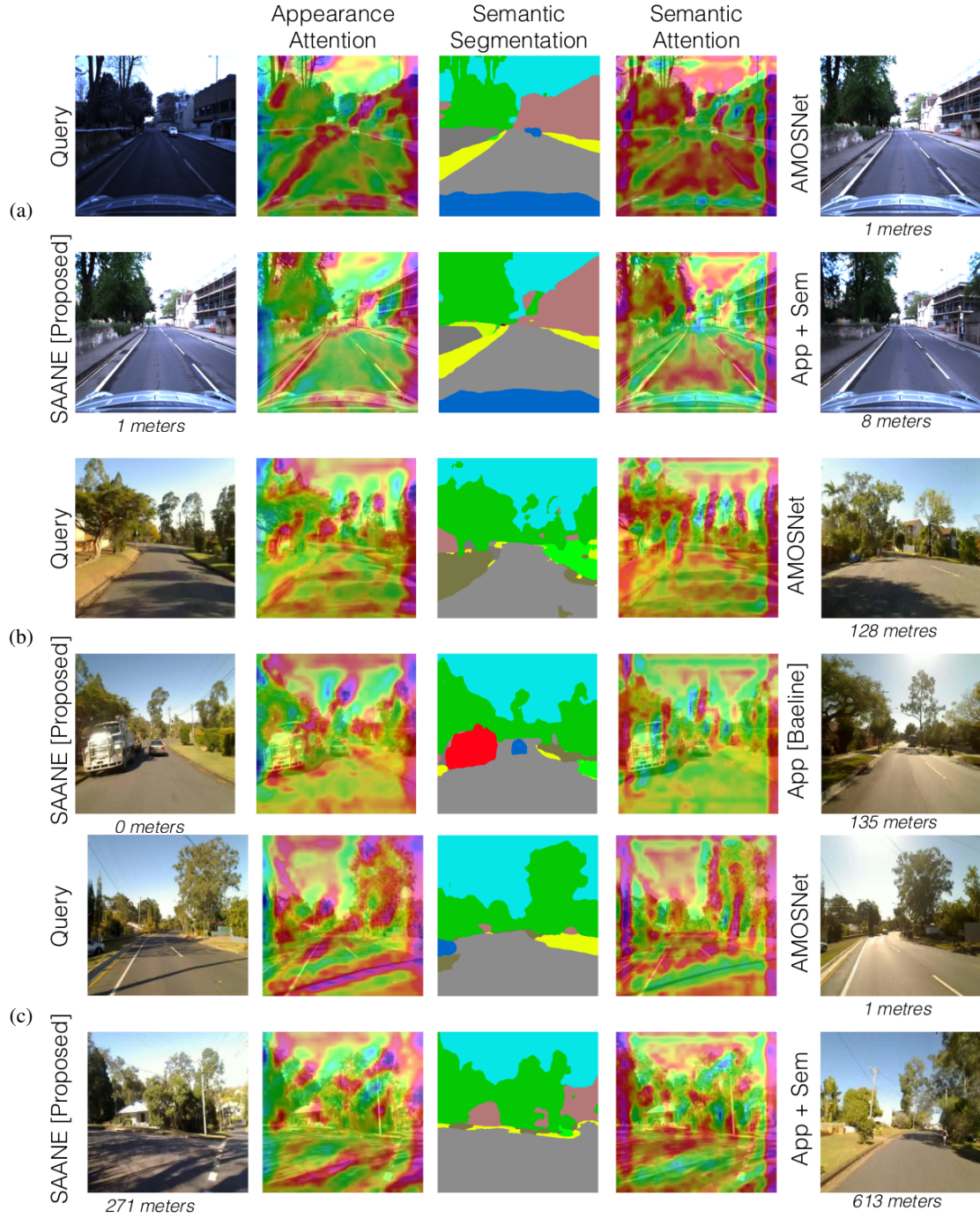


Figure 6: We present retrieval results for two successful retrieval examples under milder appearance variations from (a) RobotCar Sum.→Win., and (b) St. Lucia, to evaluate the quality of the our model and visualize the attention maps. We show a query image, database image retrieved using different methods, predicted attention maps, and the pre-computed semantic segmentation. The figure highlights that our model is able to retrieve the correct sample with and also produces attention maps that are consistent across extreme appearance changes. A failure case is shown in (c). The palette for semantic segmentation is derived from ADE20K, as follows: `skyscraper`, `sky`, `building`, `tree`, `wall`, `grass`, `sidewalk`, `car`, `plant`, `person`, `earth`, `fence`, `signboard`, `pole`, `streetlight`, `truck`, `conveyer`, `mountain`, `floor`, `van`. Figure best viewed in color.